J Solid State Electrochem (2010) 14:1401–1413
DOI 10.1007/s10008-009-0952-9

ORIGINAL PAPER

The influence of the conditions of the anodic formation and the thickness of Ag(I) oxide nanofilm on its semiconductor properties

Alexander Vvedenskii · Svetlana Grushevskaya · Dmitrii Kudryashov · Sergei Ganzha

Received: 2 September 2009 / Revised: 5 October 2009 / Accepted: 6 October 2009 / Published online: 11 November 2009

Abstract The anodic formation of Ag(I) oxide nanofilms on polycrystalline silver and Ag–Au alloys as well as on low-index single crystals of silver in 0.1 M KOH was examined. By the methods of photocurrent i_{ph} and photopotential E_{ph} measurements, the n-type conductivity of Ag_2O film was established. Since the film (6–120 nm) is thinner than the space charge region, the dependence of photocurrent and photopotential appears on the film thickness L: $i_{ph} \sim L$ and $E_{ph} \sim L^2$. The transition from polycrystalline silver to single crystals as well as the addition of a small amount of gold ($X_{Au} \leq 4$ at.%) into the silver lattice decreases the degree of deviation from the stoichiometric composition Ag_2O. The parameters of Ag_2O film (optical absorption coefficient α, donor defects concentration N_D, space charge region W, and Debye's length of screening L_D) depend on the index of a crystal face of silver, volume concentration of gold X_{Au} in the alloy, and film-formation potential E. At E=0.52 V, the sequences of variation of these parameters correlate with the reticular density sequence. The growth of the potential disturbs these sequences. The band gap in Ag_2O formed on Ag_{poly}, Ag_{hkl}, and Ag–Au is 2.32, 2.23, and 2.19 eV. Flat band potential in Ag(I) oxide, formed on Ag_{poly} in 0.5 M KOH is 0.37 V. The appearance of the clear dependence between the state of the oxide/metal interface and the structure-sensitive parameters of semiconductor Ag(I) oxide phase allows considering the anodic formation of Ag_2O on Ag as a result of the primary direct electrochemical reaction, not of the precipitation from the near-electrode layer.

Keywords Anodic oxide formation · Nanofilm · Silver · Silver–gold alloys · Photocurrent · Photopotential

A. Vvedenskii (✉) · S. Grushevskaya · D. Kudryashov · S. Ganzha
Department of Physical Chemistry, Voronezh State University, Universitetskaya pl. 1,
Voronezh 394006, Russia
e-mail: alvved@chem.vsu.ru

Introduction

The electrode processes, the oxide formation, in particular, are very sensitive to the state of the metal/solution interface predetermined, first of all, by the electrode crystalline structure, its chemical composition, as well as the potential and the nature of the electrolyte. The $Ag|OH^-(H_2O)$ system is typical in this context. It has been reliably established [1–8] that Ag_2O is the main stable product of the first one-electron stage of silver oxidation. The formation potentials of Ag(I) and Ag(II) oxides noticeably differ. Hence, it is possible, varying the potential, to examine the kinetics of the growth of namely Ag(I) oxide, while AgO or $Ag(OH)_2$ formation is thermodynamically excluded.

The role of the index of a crystal face of silver in the OH^- adsorption and initial stages of the Ag_2O growth is discussed in [9–12]. In accordance with [10], the potential of the beginning of silver oxidation shifts to positive values in the following sequence: [110]<[100]<[111]. Only for the face [110] is the clear peak on the voltammogram revealed. The authors [10] interpret this peak as a pre-phase oxidation not reaching one monolayer. This points to the enhanced reactive activity of this face with respect to OH^-, which correlates with the results [11, 12] on the electroreduction of oxygen in alkaline solution and the data of our quantum–chemical calculations [13, 14] on the highest energy of Ag_{110}–$OH_{(ads)}^-$ bond.

The role of chemical irregularity of silver surface, modeled by adding to silver the atoms of another metal, has been examined in a less degree. Gold is considered the most suitable metal for a number of reasons: Ag–Au system is a continuous series of solid solutions; the atomic radii of Ag and Au are very close, and gold is thermodynamically stable at the potentials of Ag(I) oxide formation.

It was shown [15–18] that the active dissolution of silver from Ag–Au alloys is controlled by interdiffusion of Ag and Au atoms in the alloy surface layer. However, at the potentials of Ag_2O formation, the mass transport in the oxide phase becomes the rate-controlling stage [19–21]. The anodic potential of Ag_2O formation shifts to positive values with the growth of gold concentration in the alloy. This fact is assumed to be connected with the initial stage of dealloying [21], preceding the oxide formation, resulting in the surface enrichment by gold.[1]

Hence, the essential role of the crystal structure and chemical composition of the substrate surface in the kinetics of the anodic silver oxidation at the potentials of Ag_2O formation is considered to be reliably established. The less-clear question is connected with the degree and the manner of the revealing of the kinetic features of Ag_2O formation, caused by the type of crystal face, gold concentration in the alloy, and the formation potential in the oxide properties, first of all, the semiconductor properties measured in situ. Now the problem of "size factor" arises in the first place, especially actual for nanofilms, where the properties change with the thickness [24–27] and hence, with the kinetic characteristics of the process, the conditions of the film growth, etc. These issues are poorly examined because of the difficulties of determining the partial rates of the processes simultaneously proceeding at the film-formation potentials:

1. oxide formation,
2. metal dissolution via the pores of an oxide layer,
3. chemical dissolution of an oxide phase.

The list of structure-sensitive in situ methods of investigation of oxide films is also short; among them, the spectroscopy of photocurrent (PC) and photopotential (PP) occupies an important place [28–32]. Some aspects of these investigations connected with the correlation between the film thickness L and space charge region, the correct estimation of the film thickness, and the interpretation of the photopotential relaxation after the polarization switching off, revealed by us earlier [33–35], remained outside the scope of the research.

The second, the more serious problem closely connected with the problem discussed above, concerns the mechanism of the formation of an oxide phase on the electrode, either by a direct primary electrochemical growth [3, 8] or via the stages of dissolution/precipitation (upon reaching the dissolution limit) [5, 12]. In our opinion, the revealing of a clear interdependence between structure-sensitive parameters of the oxide nanofilm and the substrate characteristics can be a strong argument in favor of the primary oxide growth.

The aim of the work is to establish the character of influence of a silver crystal face, the addition of a small amount of gold, the film-formation potential, and the concentration of hydroxide ions in the solution on the properties of the anodic Ag(I) oxide nanofilms and, on this basis, to define more accurately the oxide formation route.

Experimental

Single silver crystals and polycrystalline alloys with 1–15 at.% of gold were prepared from Ag (99.99 wt.%) and Au (99.99 wt.%). The composition and structure of electrodes were monitored by X-ray fluorescence and metallographic analysis. Single crystalline electrodes were grown in a horizontally moving furnace (2 mm/h) at temperatures from 1,273 to 673 K with the subsequent cooling during 24 h.

The surface of the electrodes was mechanically ground on grain paper with subsequently decreasing size of the abrasive, polished with water–MgO suspension on suede and rinsed with double-distilled water.

The state of the surface was monitored using the Scanning Electron Microscopy (SEM) (JSM-6380LV) and Atomic Force Microscopy (AFM) (Solver P47-PRO) methods. The chemical composition of the alloy surface layer was monitored by XP-block of the Auger microscope HB-100 (Vacuum Generators, GB) with use of Al-anode (1,486.6 eV; radiation intensity of 200 W) and the source of Argon ions AG62 with accelerating voltage of 2.3 kV and current of 60 μA cm^{-2}. X-ray Photoelectron Microscopy (XPS) measurements showed that the surface composition practically does not change as compared with volume one after the treatment described above. Indeed, after the Ag4Au alloy surface had been prepared for the experiment, the concentrations of Ag and Au were 96 and 4 at.%, respectively.

Single crystals were mechanically polished with water–MgO suspension and, additionally, chemically polished with HCl-containing saturated chromic acid solution. Before the beginning of the measurements, the state of the electrode surface was electrochemically standardized by a cathodic activation at E=−0.2 V.

The solutions 0.1 and 0.5 M reagent-grade KOH were prepared from double-distilled water and deoxygenated in the cell by passing the chemically pure argon.

The electrochemical cell was added with a quartz window at the bottom (1 mm thick). In the electrochemical

[1] The evidence of enrichment of the surface of Ag–Au alloy with gold during the dealloying are presented, for example, in [22, 23].

measurements the potentiostat IPC-compact was used. Counter Pt electrode and Ag/AgCl/Cl^- reference electrode were used. All potentials are referred to the standard hydrogen electrode scale.

In photoelectrochemical measurements, the light-emitting diodes «NICHIA» and «LIGITEK» (λ=385–875 nm) were used as a source of rectangular light pulses with the duration τ=2 ms and the repetition frequency ν= 5 Hz. The use of the earthed work electrode, a low-noise amplifier with an active filter of the fifth-order frequency and a digital signal processing (PowerGraph 2.0) made it possible to reduce the noise level to 1–2 μV. Photocurrent was measured in the regime of potentiostatic polarization; photopotential was measured in the regime of an open circuit. The sensibility of measurements was about 10 nA for photocurrent and 2–3 μV for photopotential.

The specific feature of the environment [36, 37] for PC and PP measurements in the regime discrete spectroscopy was the possibility of instantaneous and independent control of the light pulse parameters (τ, ν, and density of light flow Φ_0). We calculated the values of Φ_0 by the density of the optical power P linearly connected with the current of power supply of a light-emitting diode. The bolometer IMO-2 N was used to perform the relevance calibration.

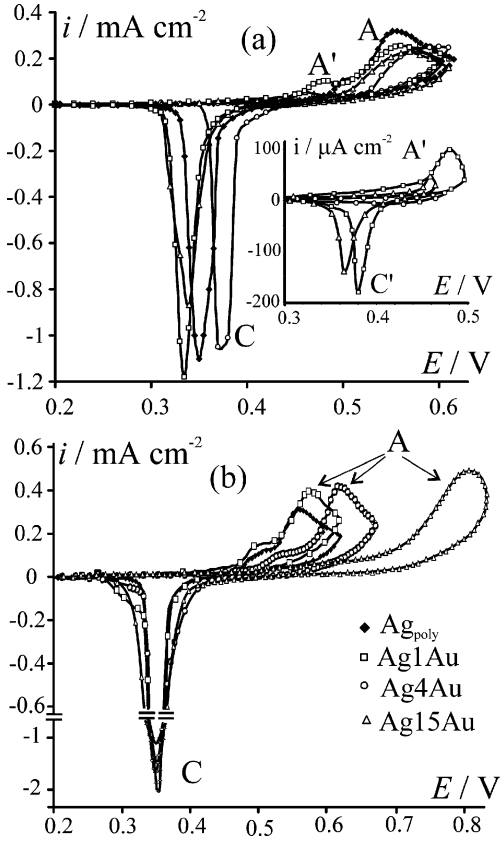

Fig. 1 Cycle voltammograms of silver **a** and Ag–Au alloys **b**

Results and discussion

Anodic formation of Ag(I) oxide on single silver crystals, polycrystalline silver, and Ag–Au alloys The role of a crystal face of the silver electrode is revealed already in the shape of voltammograms (Fig. 1a). At transition from polycrystalline silver to single crystals, the peak (A) of Ag (I) oxide formation is shifted to positive values by 10÷ 30 mV (it depends on the crystal face); the maximal currents decrease slightly. Besides, the anodic prepeak (A') and the relevant cathodic peak (C') are more clearly revealed on single crystals as compared with Ag_{poly}. The fragment in Fig. 1a demonstrates A' and C' peaks.

In [21–23] the appearance of the prepeak is accounted for the bilayer structure of the anodic film. The anodic process can be described in the simplest form:

$$Ag + OH^- \rightleftarrows AgOH_{ad}^- \rightleftarrows AgOH_{ad} + e^- \quad (1)$$

$$2AgOH_{ad} \rightleftarrows 2AgOH \rightleftarrows Ag_2O + H_2O \quad (2)$$

The Eq. 2 combines the stages of 2D- and (or) 3D-nucleation, the growth of nuclei, and the formation of AgOH phase with the subsequent dehydration to Ag_2O.

The addition of Au into Ag crystal lattice results in the ennoblement of E_A and $E_{A'}$ growing with gold atomic share X_{Au} (Fig. 1b). The shift of peak potentials can be attributed to the alloying, resulting in the decrease of the thermodynamic activity of silver a_{Ag} in the volume, hence, at the surface of Ag–Au alloy. The second possible reason of the shift is the decay of X_{Ag}^s during a short stage of dealloying, preceding the oxide formation and resulting in the enrichment of the surface with gold.

Indeed, the results of XPS measurements on Ag4Au alloy after the preliminary anodic oxidation at the potentials of Ag_2O formation points to slight enrichment of the surface with gold when the oxide is removed by the argon ions ($\tau \approx 120$ s; Fig. 2). It is interesting that gold is fixed at the initial stage of etching. In our opinion, it can be caused by the islet structure of silver oxide, resulting in the appearance of free parts of silver surface. Note that the correlation X_O/X_{Ag} in the oxide is not constant but monotonously decreases from 0.46 (in accordance with the stoichiometry of Ag_2O) to zero. However, since the film is not continuous, XPS signal most probably contains the response of silver substrate. Hence, it is impossible to consider these data as an evidence for the decreasing of the Ag–O correlation during the oxide formation.

The SEM data (Fig. 3a, c, d) are in agreement with AFM data (Fig. 3b); they confirm that the silver oxide anodically formed on silver and alloys is porous and consists of the

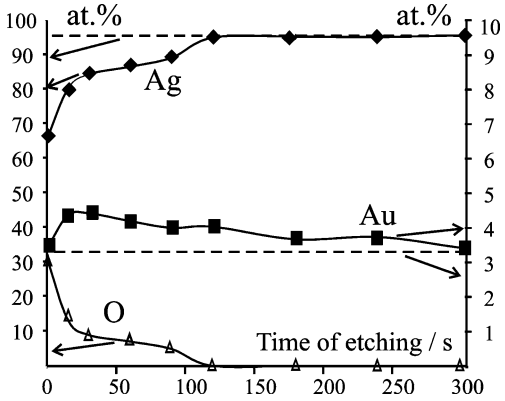

Fig. 2 The results of XPS analyze of the Ag4Au alloy surface after the anodic oxidation at E=0.60 V. The *dotted lines* show Ag and Au concentrations in the alloy without anodic oxidation after Ar^+ etching during 60 s

separate islets no more than 1 μm. The number and size of the islets decrease with the growth of gold concentration in the alloy.

The probability of self-dissolution of Ag(I) oxide in an alkaline solution [5, 6] and of silver dissolution through the defects or pores of the oxide film [7] makes it impossible to estimate the film thickness coulometrically, if there are no the data on the current efficiency ψ of oxide formation. In order to determine the current efficiency on a stationary Ag electrode after the anodic dissolution the cathodic reduction was carried out in a "fresh" solution without Ag^+ ions. It was found that the growth of polarization time of Ag_{poly} electrode (hence, the specific anodic charge q and the film thickness L) results in the initial sharp growth of the current efficiency and subsequent stabilization at the certain level not depending on the potential of oxide formation (Fig. 4a).

The transition to single crystals does not change the shape of ψ–q dependences, however, the values of ψ slightly

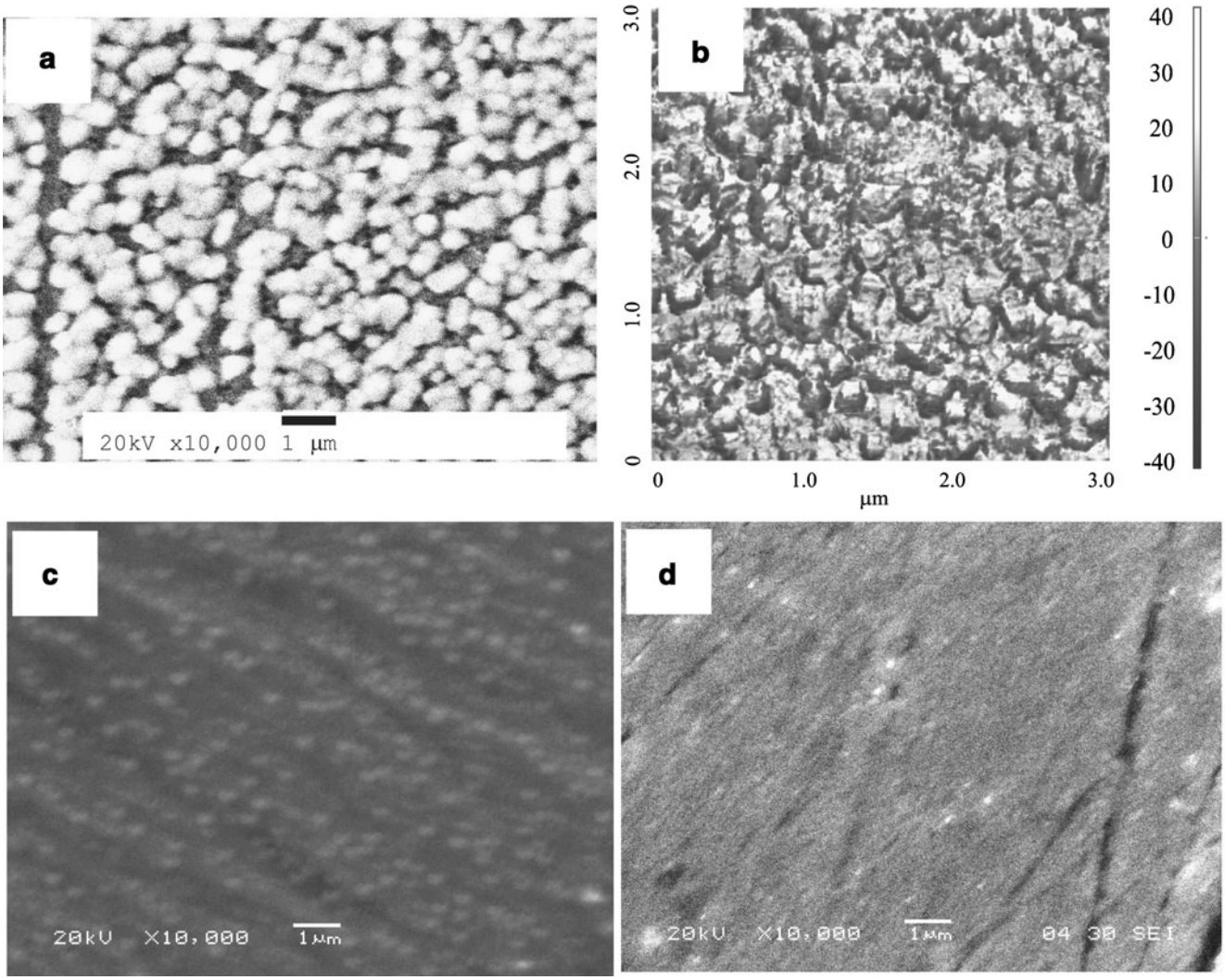

Fig. 3 SEM images (**a**, **c**, **d**) and AFM image (**b**) of the surface of Ag_{poly} (**a**, **b**), Ag4Au (**c**), and Ag15Au (**d**) covered by Ag(I) oxide with L= 120 nm formed at E=0.56 (**a**, **b**), 0.60 (**b**), and 0.77 V(**d**)

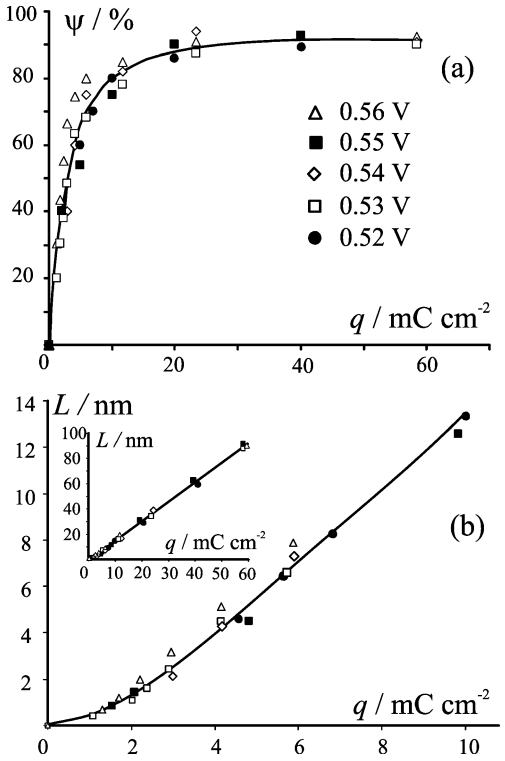

Fig. 4 The influence of anodic charge on the current efficiency of Ag (I) oxide formation on Ag_{poly} (**a**) and the film thickness (**b**)

decrease in general, which is more clearly revealed for small values of q (Table 1). On the alloys, the current efficiency is noticeably less as compared with silver. Nevertheless, a tendency of the gradual increase of the current efficiency with the anodic charge retains, pointing most probably to the decrease of porosity with the thickness.

We calculated the average thickness of the anodic film (centimeters) by the formula:

$$L = \psi \frac{A_{Ag_2O} \times Q}{zFS\rho} = \psi \frac{A_{Ag_2O}}{zF\rho} \times q, \qquad (3)$$

Where Q is overall charge; A_{Ag_2O} is molar weight of Ag_2O (232 g mol^{-1}); z=2; F=96,500 Cmol^{-1}; S is the visible electrode surface (square centimeters); ρ is the density of Ag_2O (7.14 g cm^{-3}).

The values of average thickness of Ag_2O on silver as well as on Ag–Au alloys did not exceed 150 nm (Fig. 4b). However, L is noticeably less in fact, since in calculations by (3) we did not take into account the roughness factor of the polished surface of silver and alloys. The latter is usually equal to 1.7–1.9 [38, 39].

The appearance of ψ–q dependence causes the non-linearity of L–q dependence, which often is out of scope in coulometric analysis of the average thickness of thin oxide layers. This effect is especially significant for small specific charge and hence, for small thickness (Fig. 4b). When the value of q grows and the value of ψ stabilizes, the dependence of the average thickness on the charge becomes practically linear (Fig. 4b, fragment).

Photocurrent and photopotential in anodically formed Ag (I) oxide The equations for photocurrent and photopotential processing are usually presented for semiconductor structures with thickness L exceeding the space charge region W [30]. The problem of stationary diffusion–migration distribution of the majority and minority carriers in an n-type semiconductor is solved under the following assumptions: donors are completely ionized, a semiconductor zone beyond the space charge region is quasi-neutral, the distribution of n and p in the space charge region in equilibrium state satisfies Boltzmann law, the recombination of carriers in the space charge region during the radiation does not occur. In the case of a thick semiconductor film ($L \geq W$) the initial system of equations has the form [20]:

$$\frac{d}{dx}\left[\frac{dp(x)}{dx} + p(x)\frac{d\psi(x)}{dx}\right] = -\alpha a_1 e^{-\alpha x} (0 \leq x \leq W), \qquad (4)$$

$$\frac{d}{dx}\left[\frac{dn(x)}{dx} + n(x)\frac{d\psi(x)}{dx}\right] = -\alpha a_2 e^{-\alpha x} (0 \leq x \leq W), \qquad (5)$$

Table 1 Current efficiency ψ of Ag(I) oxide formation, and the film thickness L

q/mCcm^{-2}	E=0.56V				$Ag1Au_{poly}$ (E=0.57V)	$Ag4Au_{poly}$ (E=0.60V)	$Ag15Au_{poly}$ (E=0.77V)
	Ag_{poly}	Ag_{100}	Ag_{110}	Ag_{111}			
2	71/2.4	50/1.7	47/1.6	60/2.0	33/1.1	45/1.5	40/1.3
3	73/3.7	58/2.9	56/2.8	70/3.5	41/2.1	64/3.2	47/2.4
4	79/5.3	76/5.1	63/4.2	76/5.1	60/4.0	65/4.4	46/3.1
5	83/6.7	89/7.5	69/5.8	82/6.9	65/5.5	66/5.6	58/4.9
7	85/10.0	90/10.6	77/9.1	83/9.8	72/8.5	70/8.2	64/7.5

Current efficiency values are presented as percentage of Ag(I) oxide formation (nominator) and the film thickness L, in nanometers (denominator)

$$\frac{d^2\psi(x)}{dx^2} = -\frac{e^2}{\varepsilon\varepsilon_0 kT}\left[p_0 e^{-\psi(x)} + N_D - n_0 e^{\psi(x)} - N_A\right] (0 \le x \le W), \quad (6)$$

$$\frac{d^2 p(x)}{dx^2} = -\alpha a_1 e^{-\alpha x} + \frac{p(x) - p_0}{L_p^2} (W \le x \le L). \quad (7)$$

Here n_0 and p_0 are intrinsic concentration of electrons and holes; N_D is a volume concentration of donor defects; α is a coefficient of optical absorption; $a_1 = \overline{\eta}\Phi_0/D_p$, $a_2 = \overline{\eta}\Phi_0/D_n$, where D_p and D_n are the concentration of diffusion of electrons and holes; Φ_0 is a light flux density; $L_p = (D_p\tau_p)^{1/2}$ is a diffusion length; τ_p is an average lifetime of holes. The parameter $\overline{\eta} = \eta f\left(1 - R_{ref}^{out}\right)\left(1 + R_{ref}^{in} e^{-\alpha L}\right)$ is expressed via the inner quantum efficiency η and coefficient $f = \vec{k}_{ec}/\left(\vec{k}_{ec} + \tau_p^{-1}\right)$, taking into account the difference in the rates of recombination of holes and their consumption in the electrochemical reaction at the oxide/solution interface, characterized by the rate constant $\vec{k}_{ec}$[40]. Besides, $\overline{\eta}$ takes into account the possibility of the light flux refraction from the inner oxide boundary (with respect to the substrate) as well as from the outer boundary [41]. The relevant refraction coefficients are denoted by R_{ref}^{out} and R_{ref}^{in}. Dimensionless electric potential is given by the equation:

$$\psi(x) = \frac{e\varphi(x)}{kT} = -\frac{1}{2L_D^2}\begin{cases} (x-W)^2 & L \ge W \\ (x-L)^2 + \left(W^2 - L^2\right), & L < W \end{cases} \quad (8)$$

where $\varphi(x; t)$ is a local electric potential in the oxide film; $L_D = (\varepsilon\varepsilon_0 kT/e^2 N_D)^{1/2}$ is Debye's length and ε is a dielectric constant of the oxide. The properties of the oxide are considered constant along its thickness.

For thin films with a thickness less than a space charge region ($L<W$) the Eq. 7 is redundant and the solution of Eqs. 4–6 is processed in an interval $0 \le x \le L$. Let us show the final equations obtained in [20] for photocurrent and photopotential in a thin film with a high enough level of light absorption, when $\alpha L_D \ge 1$:[2]

$$i_{ph} = e\eta f\Phi_0\left(1 - R_{ref}^{out}\right)\left(1 + R_{ref}^{in} e^{-\alpha L}\right)\left(1 - e^{-\alpha L}\right) + \frac{eN_D D_n\left(1 - e^{-\frac{eE_{ph}}{kT}}\right)}{\sqrt{2}L_D F\left(L/\sqrt{2}L_D\right)} \exp\left\{-\frac{e\left(E - E_{fb}\right)}{kT}\right\}, \quad (9)$$

$$E_{ph} = -\frac{kT}{e}\ln\left[1 + \frac{\eta f\Phi_0\left(1 - R_{ref}^{out}\right)\left(1 + R_{ref}^{in} e^{-\alpha L}\right)\left(1 - e^{-\alpha L}\right)}{N_D D_n} L_D\sqrt{2}F\left(\frac{L}{\sqrt{2}L_D}\right)\exp\left\{\frac{e\left(E - E_{fb}\right)}{kT}\right\}\right]. \quad (10)$$

Here, E is the oxide-formation potential, E_{fb} is flat band potential, and $F(u)$ is an integral of Doson. Let us assume that it is not the appearance of photopotential but the generation of electron-hole pairs that makes a main contribution to the photocurrent. Let us consider $R_{ref}^{in} \approx 1$, and the second term in brackets under the logarithm is small as compared with unity. Taking into account $F(u) \approx u$ at $L/\sqrt{2}L_D < 1$, one can obtain under obvious assumptions:

$$i_{ph} = e\eta f\Phi_0\left(1 - R_{ref}^{out}\right)\left(1 - e^{-2\alpha L}\right) = i_{ph}^{max}\left(1 - e^{-2\alpha L}\right) \approx 2\alpha i_{ph}^{max} L, \quad (11)$$

$$E_{ph} = -\frac{2kT}{e} \times \frac{\eta f\Phi_0\left(1 - R_{ref}^{out}\right)\alpha L^2}{N_D D_n}\exp\left\{\frac{e\left(E - E_{fb}\right)}{kT}\right\}. \quad (12)$$

It follows from Eqs. 11 and 12 that PC and PP dependence on Φ_0 is linear at low enough light intensity. However, the influence of the film thickness on the photosignal parameters for thin film alters: $i_{ph} \sim L$ and $E_{ph} \sim L^2$. Note that, for thick films, such an influence is absent.

Photocurrent A typical chronoammogram of Ag_2O formation on polycrystalline silver is characterized by a fast decay of the anodic current (Fig. 5). In the initial period of potentiostatic polarization (5–7 s), the photocurrent is not registered or does not exceed the noise level. However, starting from a certain time, corresponding to the formation of the oxide film with a significant thickness, the pulse illumination results in the synchronous arising of pulses of the anodic photocurrent (Fig. 5, fragment). The appearance of the anodic photocurrent at the potential greater than the flat band potential[3] points to n-type conductivity of semiconductor oxide on Ag_{poly} [28, 29]. The existence of free electrons can be attributed to the prevalence of superstoichiometric Ag atoms or oxygen vacancies in Ag_2O crystal lattice. According to the data in [19], the Ag^+-ion transport through Ag_2O film determines the kinetics of

[2] The numerical analysis shows that in thin films with a low level of light absorption ($\alpha L_D << 1$), PP and PC values are negligibly small.

[3] In a special set of experiments, the dependence of the capacity of Ag_{poly}/0.5 M KOH boundary on the potential was obtained. The extrapolation in the coordinates of Mott–Schottky gives the value of flat band potential for Ag_2O E_{fb}=0.37 V in accordance with [42], where E_{fb}=0.33 V

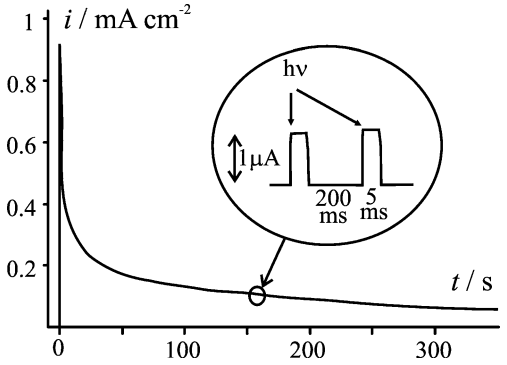

Fig. 5 Chronoammogram of Ag_{poly} electrode in 0.1 M KOH at E=0.56 V

oxide formation. Therefore, it is reasonable to assume, that the super-stoichiometric Ag atoms determine the defectiveness of the oxide. Hence, the composition of the oxide can be described by the formula $(Ag_{Ag})_2(Ag_i)_\delta O_O$.

In accordance with Eq. 11, the photocurrent amplitude increases with the growth of charge and with the thickening of the oxide film, reaching the limiting level $i_{ph}^{max} = e\eta f\Phi_0\left(1 - R_{ref}^{out}\right)$ (Fig. 6a). The shape of i_{ph}–L dependence does not change in general with a variation of the Ag_2O formation potential. Nevertheless, i_{ph} slightly increases with E, which is especially noticeable at peak potential (0.56 V).

Theoretical curves, calculated by Eq. 11 (dotted lines in Fig. 6), are in agreement with the experimental data, which makes it possible to calculate the coefficient α and product $\eta f(1\text{-}R_{ref}^{out})$ (Table 2). The values of W are obtained by extrapolating i_{ph}-t dependence to the value of i_{ph}^{max}, corresponding to the lack of influence of thickness on the photocurrent and to the condition $i_{ph}(L)/i_{ph}^{max}$=0.99. Assuming that ε_{Ag_2O}=11 for thin Ag_2O films [43], we obtained N_D by the formula $W = \left(2\varepsilon\varepsilon_0\left|E - E_{fb}\right|/eN_D\right)^{1/2}$ and then calculated L_D and αL_D.

The values of i_{ph}^{max} and $\eta f(1\text{-}R_{ref}^{out})$ do not practically depend on the potential of Ag_2O formation (Table 2). If we assume η =1 and f=1, then we formally obtain a very high value of R_{ref}^{out} ~0.9926, which is hardly probable. Most likely f<<1 because of a low rate of the electrochemical process of hole assimilation at the oxide/solution interface as compared with the rate of their volume or surface recombination.

It follows from Fig. 6 and Table 2 that L<W. However, since L_D is 3÷4 times less than the space charge region, the correlation between L and L_D can be both greater and less than unity, depending on the film thickness. The latter is compared with the depth of optical absorption α^{-1}, which means that the entire oxide phase is optically active.

At the same film thickness and formation potential, the photocurrent in Ag_2O on single Ag crystals is always less than the photocurrent in Ag_2O on Ag_{poly} substrate (Fig. 6b). The dependences of photocurrent on the thickness of Ag_2O

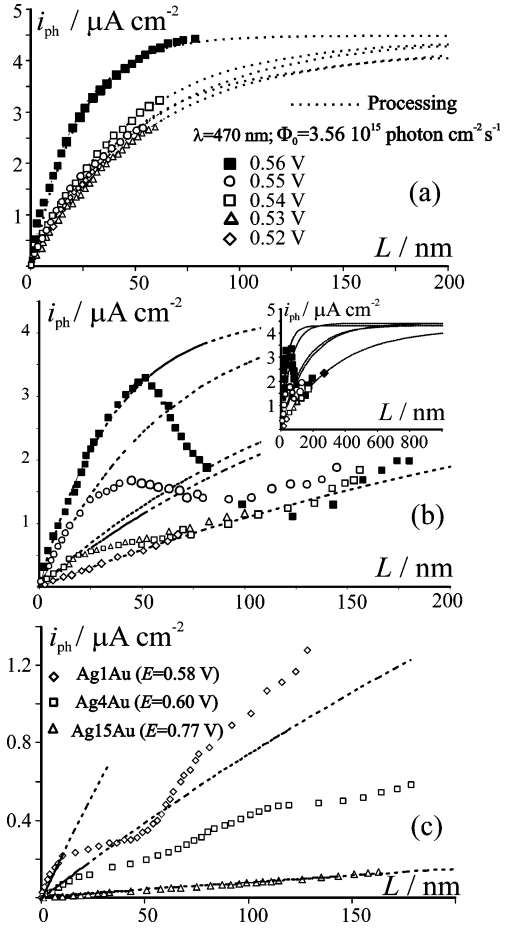

Fig. 6 The dependence of photocurrent on the Ag(I) oxide thickness on Ag_{poly} (**a**), Ag_{100} (**b**), and Ag–Au alloys (**c**); the relevant theoretical dependence, calculated using Eq. 11, is presented as a *dotted line*

films, formed at E=const on different faces of Ag single crystals, are similar in shape, if the films are thin. However, their character changes with the film-formation potential. At low potentials (E=0.52÷0.54 V), the photocurrent monotonously grows with Ag_2O film thickness. At higher potentials (E=0.55÷0.56 V) the initial growth of photocur-

Table 2 The dependence of structural and optical characteristics of Ag_2O on the potential of oxide formation on Ag_{poly} at λ=470 nm and Φ_0=3.56×10^{15} photon s^{-1}cm^{-2}

Parameter	0.52V	0.53V	0.54V	0.55V	0.56V
i_{ph}^{max}/μA cm^{-2}	4.4	4.2	4.3	4.0	4.4
$\eta f(1-R_{ref}^{out})\times10^4$	77	73	75	70	77
$\alpha\times10^{-5}$/cm^{-1}	0.90	0.90	1.08	1.10	2.30
α^{-1}/nm	111	111	93	91	43.5
W/nm	256	256	213	209	100
$N_D\times10^{-15}$/cm^{-3}	2.83	2.98	4.51	4.90	22.4
L_D/nm	74.3	72.5	58.9	56.5	26.4
αL_D	0.67	0.65	0.63	0.62	0.61

Table 3 The parameter $\eta f(1-R_{ref}^{out})$, the absorption coefficient (at λ=470 nm), and the space charge region in Ag(I) oxide formed on single crystalline silver

E/V	$\eta f(1-R_{ref}^{out})\times10^4$			$\alpha\times10^{-5}$/cm^{-1}			W/nm		
	Ag_{110}	Ag_{100}	Ag_{111}	Ag_{110}	Ag_{100}	Ag_{111}	Ag_{110}	Ag_{100}	Ag_{111}
0.52	70	74	72	0.08	0.12	0.13	2,875	1,917	1,769
0.53	77	77	75	0.11	0.30	0.13	2,091	767	1,769
0.54	72	75	74	0.06	0.35	0.18	3,833	657	1,278
0.55	75	77	75	0.38	0.8	0. 8	605	288	288
0.56	77	75	79	0.7	1.4	1.0	329	164	230

rent is followed by its decay.[4] The maximum of PC shifts to a greater thickness in the sequence $Ag_{100} \rightarrow Ag_{111} \rightarrow Ag_{110}$. In this case, the initial section of i_{ph}–L dependence was used for a numerical analysis of α and i_{ph}^{max} by Eq. 11 for single crystals. The results of calculation are presented in Tables 3 and 4.

The parameter $\eta f(1\text{-}R_{ref}^{out})$ practically does not depend on the face of single Ag crystal and the film-formation potential. Moreover, the values of this parameter coincide with that presented in Table 2 for polycrystalline silver. At the same time, the optical absorption coefficient α in Ag(I) oxide, formed on a single crystalline substrate, is sufficiently less as compared with a polycrystalline substrate. The growth of the potential in an interval 0.52÷0.54 V slightly influences α. Nevertheless, the further increase of the potential by 10 mV causes a sharp enough increase of the absorption coefficient, proving a significant structural change of the forming oxide and indirectly confirming the bilayer structure of the oxide film.

The space charge region W in Ag(I) oxide, obtained at low potentials on single crystals, is sufficiently, almost by an order, greater than in the case of a polycrystalline substrate. The decrease of W with the oxide-formation potential, revealed for a polycrystalline substrate, retains and becomes clearer.

The concentration of donor defects in Ag(I)oxide, formed on single silver crystals, is almost ten times less than in Ag(I) oxide, formed on polycrystalline silver. Respectively, the degree of deviation from the stoichiometric composition Ag_2O decreases from $\delta=120\times10^{-8}$ for $Ag_2O|Ag_{poly}$ to $\delta=1\div45\times10^{-8}$ for $Ag_2O|Ag_{hkl}$ systems. The growth of the anodic potential of Ag(I) oxide formation leads to the increase of the degree of structure disordering of the oxide phase. The analogous tendency characterizes the change of Debye's length: independent of the crystal face, the values of L_D decrease in general with the growth of E. At low potentials, L_D in the oxide on single crystals is noticeably greater as compared with a polycrystalline substrate. It is demonstrative that the product αL_D, slightly decreasing with the potential, coincides with that obtained for Ag(I) oxide formed on Ag_{poly} (Table 2).

Thus, the parameters of anodically formed Ag(I) oxide depend not only on the face of a single Ag crystal but on the film-formation potential as well. Only at E=0.52 V, corresponding to the least (among the reviewed) shift of the potential from $E_{Ag|Ag_2O|OH^-}^{eq}$, we can set the following sequences:

$$\begin{aligned}
&\alpha(Ag_2O/Ag_{110}) < \alpha(Ag_2O/Ag_{100}) < \alpha(Ag_2O/Ag_{111})\\
&N_D(Ag_2O/Ag_{110}) < N_D(Ag_2O/Ag_{100}) < N_D(Ag_2O/Ag_{111})\\
&W(Ag_2O/Ag_{110}) > W(Ag_2O/Ag_{100}) > W(Ag_2O/Ag_{111})\\
&L_D(Ag_2O/Ag_{110}) > L_D(Ag_2O/Ag_{100}) > L_D(Ag_2O/Ag_{111}),
\end{aligned} \tag{13}$$

that correlate with the change of a reticular density of crystal faces: [110]<[100]<[111]. The growth of the potential disturbs these sequences:

$$\begin{aligned}
&\alpha(Ag_2O/Ag_{100}) < \alpha(Ag_2O/Ag_{111}) < \alpha(Ag_2O/Ag_{110})\\
&N_D(Ag_2O/Ag_{100}) < N_D(Ag_2O/Ag_{111}) < N_D(Ag_2O/Ag_{110})\\
&W(Ag_2O/Ag_{100}) > W(Ag_2O/Ag_{111}) > W(Ag_2O/Ag_{110})\\
&L_D(Ag_2O/Ag_{100}) > L_D(Ag_2O/Ag_{111}) > L_D(Ag_2O/Ag_{110}),
\end{aligned} \tag{14}$$

Chemical composition of the substrate is also a sufficient factor, influencing the properties of Ag(I) oxide. Ag (I) oxide films formed on Ag–Au alloys at the peak potentials of i–E(t) dependence are characterized, in general, by lower amplitudes of photocurrent, decreasing with the growth of gold concentration in the alloy (Fig. 6c). The character of the photocurrent–thickness dependence is rather complicated. Hence the optical and structural parameters of Ag(I) oxide formed on the Ag–Au alloys were calculated by the initial section of i_{ph}–L dependence (Table 5), as was the case in the experiments with single crystals.

The growth of X_{Au} results in a sharp decrease of α coefficient, the space charge region significantly increases and the concentration of donor defects in the oxide film noticeably decays (Table 5). It means that Ag_2O film formed on Ag–Au alloys is more stoichiometric than the film formed on pure silver, which is rather unexpected. The degree of deviation from the stoichiometric composition decreases to $\delta = 0.3 \div 2.2 \times 10^{-8}$.

[4] The problem of i_{ph} decay in Ag(I) oxide on Ag_{hkl} after the film thickness achieves 50 nm needs further investigation in detail.

Table 4 Donor defects concentration, Debye's length of screening, and the parameter αL_D in Ag(I) oxide formed on single crystalline silver

E / V	$N_D \times 10^{-14}/cm^{-3}$			L_D/nm			αL_D		
	Ag_{110}	Ag_{100}	Ag_{111}	Ag_{110}	Ag_{100}	Ag_{111}	Ag_{110}	Ag_{100}	Ag_{111}
0.52	0.224	0.50	0.591	837	559	515	0.67	0.67	0.67
0.53	0.445	3.31	0.622	593	217	502	0.65	0.65	0.65
0.54	0.139	4.73	1.25	1061	182	354	0.64	0.64	0.64
0.55	5.85	25.9	25.9	163	78	78	0.62	0.60	0.62
0.56	20.7	83.0	42.3	87	43	61	0.61	0.60	0.61

The parameter $\eta f(1\text{-}R_{ref}^{out})$ is the same as for Ag_2O films formed on poly-silver crystals and single silver crystals. Debye's length L_D, being less than W, noticeably grows with X_{Au}. The product αL_D remains close to unity, which makes it possible to consider the film formed on alloys as a semiconductor with a high absorption of light at λ=470 nm.

Photopotential After switching off the polarization, the illumination of Ag_2O films of different thickness, potentiostatically formed on Ag_{poly} electrode, gives a negative photopotential (Fig. 7), pointing to an n-type conductivity. Independently of the formation potential, illumination intensity and the value of the anodic charge in the interval L=2÷200 nm, the photopotential decreases in time. The most part of E_{ph}–t dependence is linearized in the coordinates (Fig. 8), corresponding to a formal-kinetic equation of irreversible reaction of the first order:

$$\ln\left[E_{ph}(t) - E_{ph}^{st}\right] = \ln\left[E_{ph}(0) - E_{ph}^{st}\right] - \vec{k}\,t \qquad (15)$$

Here $E_{ph}(0)$ and E_{ph}^{st} are the values of photopotential at the moment of switching off the polarization and of the reaching the quasi-stationary level, $\vec{k}$ is a rate constant of the process, causing the photopotential decay.

Taking into account the dependence of photopotential on the anodic film thickness by Eq. 12 and the results obtained by us earlier in the experiments with RRDE [44], we can confidently assume that the decay of E_{ph} in time is caused by a thinning of the film in the course of its chemical dissolution in accordance with the kinetic equation $dL/dt = -\vec{k}L$.

The negative photopotential is also valid for Ag(I) oxide formed on single Ag_{100}, Ag_{110}, and Ag_{111} crystals. The shape of E_{ph}–t dependence retains (Fig. 8), though, the photopotential amplitude is lower in the whole interval of time as compared with the photopotential in Ag_2O formed on a polycrystalline substrate. Meanwhile, the transition from Ag_{poly} to Ag_{hkl} practically does not change the value of $\vec{k}$. It is clear, if one takes into account that the dissolution of Ag(I) oxide proceeds at the film/electrolyte interface, hence, does not depend on the substrate properties.

Independently of the crystal face, formation potential, light intensity, and wave length, a sufficient influence of Ag_2O film thickness on the photosignal amplitude is observed. The experimental $E_{ph}(0)$–L^2 dependence is linear (Fig. 9a) in accordance with Eq. 12; the same is valid for $E_{ph}(0)$–Φ_0 dependence (Fig. 9b).

Presenting Eq. 12 in another form

$$E_{ph} \approx -\frac{2e\Phi_0\eta f\left(1 - R_{ref}^{out}\right)\alpha L^2}{\sigma_n}\exp\left\{\frac{e\left(E - E_{fb}\right)}{kT}\right\} \qquad (16)$$

and using optical and structural parameters of the oxide film, obtained in photocurrent experiments, we calculated the partial electron photoconductivity $\sigma_n = e\mu_n n \approx e\mu_n N_D$ from the slope of E_{ph}–L^2 dependence at E=const and then the electron mobility μ_n in Ag_2O film (Table 6). In the oxide of a constant thickness formed on polycrystalline silver, the partial electron photoconductivity σ_n slightly increases with the film-formation potential. Since μ_n changes less significantly and non-systematically, we can assume that a slight growth of σ_n with E is exactly connected with the increase of the concentration of donor defects. Note, in this connection, that, in general, the photoconductivity of an n-type oxide is bipolar $\sigma = \sigma_p + \sigma_n$. However, the minority carriers (holes in our case) make the main contribution to the overall migration flux in the space charge region under illumination. However, the calculation by Eq. 16 results in the

Table 5 Optical and structural parameters of Ag_2O oxide formed on Ag–Au alloys

X_{Au}/at.%	E/V	$\alpha \times 10^{-5}/cm^{-1}$	W/nm	$N_D \times 10^{-12}/cm^{-3}$	$\eta f(1-R_{ref}^{out}) \times 10^4$	L_D/nm	αL_D
1	0.58	0.3	767	414	70	194	0.58
4	0.60	0.1	2,300	49.7	72	570	0.57
15	0.77	0.009	25,556	0.66	72	4,870	0.44

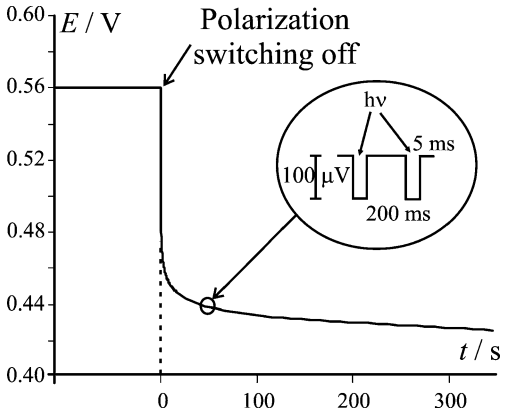

Fig. 7 Chronopotentiogram of Ag_{poly} electrode in 0.1 M KOH at q=7 mC cm^{-2}, λ =470 nm, and Φ_0=3.56×10^{15} photon s^{-1}cm^{-2}

values of σ_n, incomparable in principal with a volume conductivity of Ag(I) oxide, determined by the majority carriers.

The transition from Ag(I) oxides formed at E=0.56 V on a polycrystalline substrate to the oxides of the same thickness but formed on single crystals shows that partial electron photoconductivity slightly decreases and the electron mobility in the space charge region of the oxide increases. The order of changing of σ_n and μ_n at E=0.53÷0.56 V coincides with that established above for α, N_D, W, and L_D (the sequences (14)):

$$\sigma_n(Ag_2O|Ag_{100}) > \sigma_n(Ag_2O|Ag_{111}) > \sigma_n(Ag_2O|Ag_{110})$$
$$\mu_n(Ag_2O|Ag_{100}) < \mu_n(Ag_2O|Ag_{111}) < \mu_n(Ag_2O|Ag_{110}). \quad (17)$$

Silver oxide on Ag–Au alloys for photoelectrochemical investigations was formed at the potential of a main peak in the voltammograms. This potential shifted to positive values with the growth of gold concentration. In all cases, the photopotential is negative. The exponential character of a photopotential dependence on time after switching off the

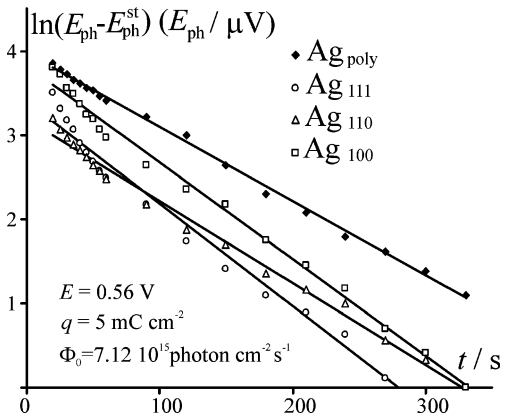

Fig. 8 Photopotential decay in time after the polarization switching off

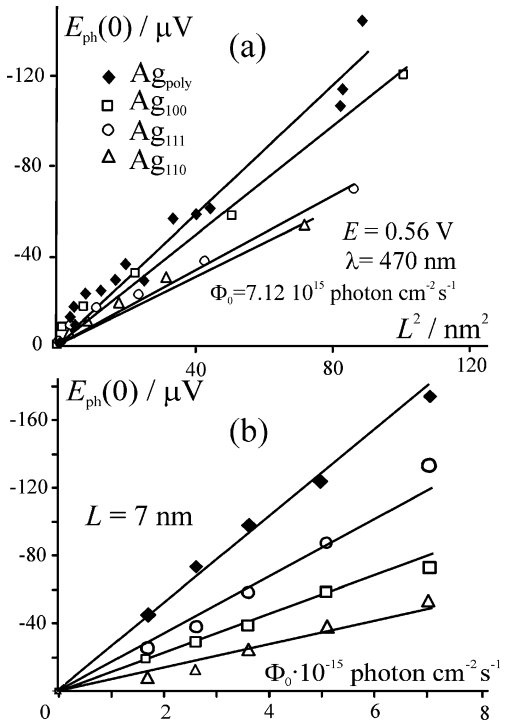

Fig. 9 The dependence of photopotential on Ag_2O thickness (**a**) and the light intensity (**b**)

polarization retains as well. The values of σ_n and μ_n are calculated from the linear part of E_{ph}–L^2 dependence (Table 6). An increase of gold concentration in a silver crystal to 4 at.% results in a decrease of the partial electron photoconductivity σ_n. A sharp increase of σ_n in the oxide on Ag15Au is hardly demonstrative, since, at the film-formation potential, E=0.77 V, the formation of AgO is possible.

The influence of OH⁻ ion concentration on the photopotential In order to define more accurately the route of the oxide formation on silver, the photopotential was measured in the solutions with different KOH concentrations. Preliminary voltammetric investigations show that the peak potentials ($E_{A'}$ and E_A) on the anodic branch shift to negative values with the growth of C_{OH^-}. However, the shift approximately coincides with the difference of equilibrium potentials of Ag_2O formation; hence, the overpotential of Ag(I) oxide formation practically does not depend on the concentration of alkaline solution. This conclusion results from a more precise analysis of the influence of OH^- concentration (0.01; 0.02; 0.05; 0.07; 0.10; and 0.20 M) on the peak potential in the nitrate–alkaline solution with the constant ionic force of 0.2 mol/dm^3. It was found that the slope of the linear dependence of the peak potential on the concentration of OH ions $dE_A/d\lg C_{OH^-}$= 0.059 V which is in accordance with the Nernst slope $dE^{eq}_{Ag_2O/Ag}/d\lg C_{OH^-}$.

Nevertheless, in the overall *i–E* dependence, the currents increase with concentration. In order to establish the reason for current growth, either the increase of the rate of the anodic oxide formation or the intensification of silver dissolution with the formation of soluble products, the values of current efficiency in KOH solutions with different concentrations were determined. It has appeared that, at all potentials, the values of ψ noticeably decrease with the growth of OH^- ion concentration. Indeed, for the oxide formation in 0.1 M KOH at the potential of the main anodic peak E_A=0.56 V, the current efficiency is equal to 83% (Table 1), while in 0.5 M KOH at the potential of the main anodic peak E_A=0.53 V, this value is reduced more than twice and is equal to 38%. Note that the specific charge was the same q=5 mC cm^{-2}. With the growth of the anodic charge from 5 to 14 mC cm^{-2}, the values of ψ in 0.5 M KOH increase from 38% to 53%, remaining low enough. One can assume that the growth of alkali concentration results in the formation of a more porous oxide layer and hence, the increase of the rate of the active silver dissolution.

The data obtained are important for the solution of the following problem: does the photopotential in anodic Ag(I) oxide depend on C_{OH^-}? The analysis of Fig. 10 shows that such dependence seems to exist: independent of the wave length the value of E_{ph} noticeably decreases with the growth of electrolyte concentration. Meanwhile, if the main parameters of Ag(I) oxide do not change with C_{OH^-}, then combining Eqs. 3 and 12, one can obtain the correlation:

$$\frac{E_{ph}(C_1)}{E_{ph}(C_2)} = \left[\frac{\psi(C_1)}{\psi(C_2)}\right]^2 \quad (18)$$

If C_1=0.1 and C_2=0.5 M KOH, then the right side of Eq. 18 is equal to 4.4. Fig. 10 shows that $E_{ph}(C_1)/E_{ph}(C_2)$ is equal in average to 3.5 and 2.9 at λ=470 and 525 nm, respectively (the specific charge in all experiments q= 5 mC cm^{-2}). Therefore, one can conclude that the decay of E_{ph} with the growth of C_{OH^-} seems, resulting from the decrease of the film thickness because of the current efficiency decrease. In fact, the E_{ph} does not depend on the electrolyte concentration. This fact allows one to assume that photoresponse arises exactly in the oxide phase not at the oxide/solution interface.

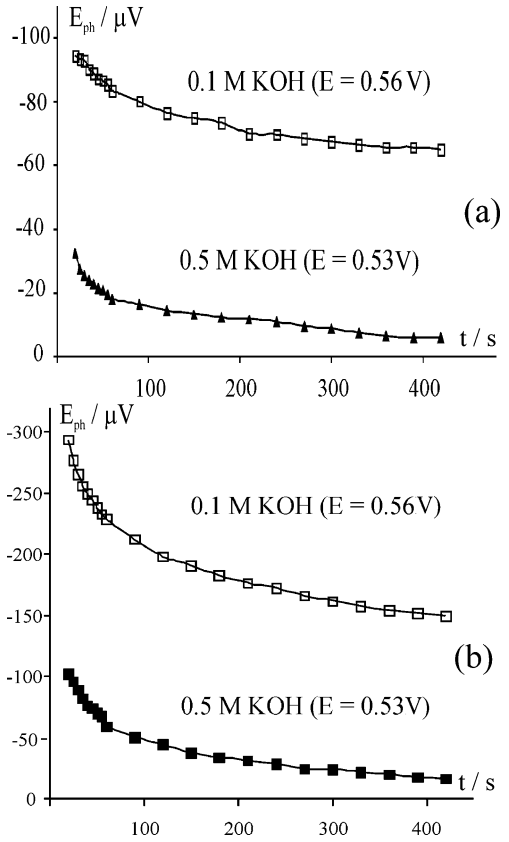

Fig. 10 Photopotential in Ag(I) oxide formed on Ag_{poly} with different KOH concentration at λ=470 (**a**) and 525 nm (**b**); q=5 mC cm^{-2}

Note that the rate constant $\vec{k}$ of the oxide chemical dissolution, obtained in the experiments with different λ (400÷629 nm), practically does not depend on the concentration of the alkaline solution, being equal to 0.008 ± 0.001 and $0.008 \pm 0.002 s^{-1}$ at $C_{OH^-} = 0.1$ and 0.5 M OH^-, respectively.

Thus, the experimentally established influence of the silver crystal face, its alloying with gold and the film thickness on the photoelectrochemical parameters in Ag (I) anodic oxide as well as the lack of such influence on the part of the electrolyte concentration show that the photopotential and photocurrent are connected with the volume but not the surface energy levels. Besides, the presence of a clear-cut dependence between the state of the oxide/solution interface and the values of all structure-sensitive parameters of Ag_2O semiconductor phase as well as the lack of interrelations between OH^-

Table 6 Partial electron photoconductivity σ_n and electron mobility μ_n in Ag(I) oxide formed on different electrodes

Electrode	Ag_{poly}			Ag_{110}	Ag_{100}	Ag_{111}	Ag1Au	Ag4Au	Ag15Au
E/V	0.54	0.55	0.56	0.56	0.58	0.60	0.58	0.60	0.77
$\sigma_n \times 10^5$/$Ohm^{-1}cm^{-1}$	2.3	3.1	9.8	4.8	2.19	0.43	2.19	0.43	222
$\mu_n \times 10^2$/$cm^2 s^{-1} V^{-1}$	3.21	3.96	2.73	14.5	33.1	53.7	33.1	53.7	–

ion concentration and Ag_2O parameters demonstrate that the anodic formation of Ag(I) oxide is mainly a result of the direct primary electrochemical growth and not the result of super-saturation of the near-electrode layer with respect to AgOH with a subsequent dehydration of the precipitate.

Photocurrent and photopotenial spectroscopy Since photocurrent and photopotential are proportional to the optical absorption coefficient α by Eqs. 11 and 12, one can obtain the similar PC and PP spectral dependence at L=const, E=const, and Φ_0=const, taking into account α–ν correlation [30]:

$$\left(i_{ph}h\nu\right)^{2/m}=C_1L^{2/m}\left(h\nu-E_{bg}\right) \quad (19)$$

$$\left(E_{ph}h\nu\right)^{2/m}=C_2L^{4/m}\left(h\nu-E_{bg}\right) \quad (20)$$

Here E_{bg} is a band gap, C_1 and C_2 are the coefficients, the parameter m is equal to 1 or 4 for direct or indirect optical transition.

The dependences of photocurrent on the film thickness at λ=385÷875 nm, E=0.56 V, and $\Phi_0=3.56\times10^{15}$ photon $s^{-1}cm^{-2}$ are similar, which makes it possible to estimate the value of coefficient α and to build its spectral dependence (Fig. 11). Most probably, the middle peak (λ=470 nm) corresponds to the range of intrinsic conductivity; the nature of additional peaks is not clear. Band gap E_{bg} in Ag_2O oxide formed on polycrystalline silver is 2.32 eV for direct optical transitions.

Spectral dependences of photocurrent generated in $Ag_2O|Ag_{hkl}$ and $Ag_2O|Ag$–Au systems are similar in shape, and they have three peaks. In the coordinates (19), they show a better linear dependence in the case of direct transitions. E_{bg} for Ag(I) oxide on Ag–Au alloys is 2.19 eV (Fig. 12a) and does not depend on the alloy composition (in the frame of experimental mistake).[5] Band gap for direct optical transitions in Ag_2O oxide formed on Ag_{hkl} is 2.23 eV, the role of the crystal face practically is not revealed.

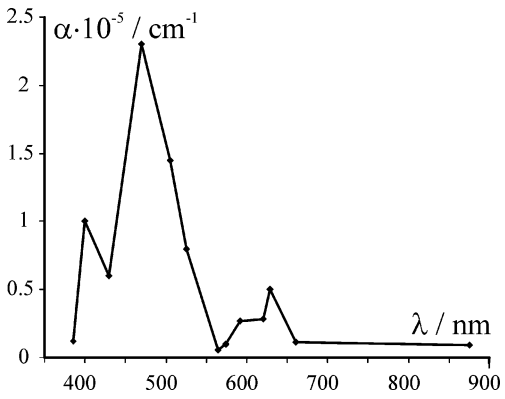

Fig. 11 Spectral dependence of the absorption coefficient in Ag(I) oxide on Ag_{poly}

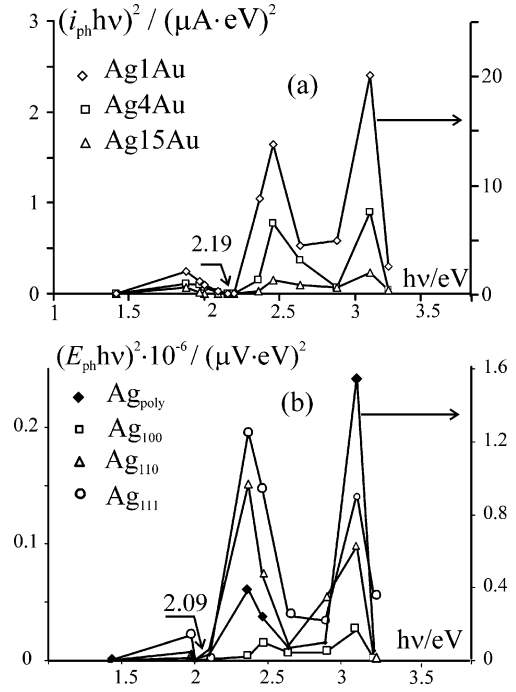

Fig. 12 Spectral dependence of photocurrent in Ag(I) oxide on Ag–Au alloys (**a**) and photopotential in Ag(I) oxide single crystals (**b**) in the coordinates criterial for direct optical transitions

Spectral dependence of photopotential in Ag_2O formed on polycrystalline silver and its single crystals is also characterized by three peaks (Fig. 12b) with the same positions as for photocurrent spectra. The graphic processing of E_{ph}–$h\nu$ dependence in criterial coordinates (20) shows that direct optical transitions prevail; however, the value of E_{bg} slightly differs from that obtained by photocurrent measurement. Band gap is equal to 2.09 eV independently from the solution concentration.

Conclusions

1. The predominant route of Ag(I) oxide anodic formation on silver is not the precipitation from the near-electrode layer, but mainly the direct electrochemical reaction.
2. The face of a single silver crystal, the chemical composition of Ag–Au alloy and the thickness of the nanofilm of the n-type semiconductor Ag(I) oxide

[5] Note that the accuracy of determination of band gap in Ag_2O oxide± 0.1 eV is low enough to draw conclusions on the influence of the crystal face and alloy composition on E_{bg}.

sufficiently influence the parameters of the photosignal generated not at the electrode/solution interface, but in the volume of the oxide phase.

3. The transition from polycrystalline silver to single crystals as well as the alloying of silver with gold up to 4 at.% result in a decrease of the degree of deviation from the stoichiometric composition Ag_2O. The growth of the potential has an opposite effect.
4. When the potential of oxide formation is low, its structure-sensitive parameters (optical absorption coefficient α, donor defects concentration N_D, space charge region W, and Debye's length L_D) change in accordance with the reticular density of atoms on the crystal face. The growth of overpotential of oxide formation disturbs these sequences.
5. The band gap in Ag(I) oxide formed on Ag_{poly} is 2.32 eV, in Ag(I) oxide formed on Ag_{hkl} is 2.23 eV, in Ag(I) oxide formed on Ag–Au alloys is 2.19 eV independently from the alloy composition (1, 4, or 15 at.% of Au). The direct optical transitions dominate in all systems at UV irradiation. Flat band potential in Ag(I) oxide formed on Ag_{poly} in 0.5 M KOH is 0.37 V.
6. The initial part of the dependence of the average thickness of Ag(I) oxide film on the anodic charge is not linear because of an essential role of silver active dissolution from the open parts of surface. The decay of photopotential in Ag(I) oxide observed at the growth of the solution concentration from 0.1 to 0.5 M seems because of the noticeable decrease of the current efficiency of the oxide formation.

Acknowledgements We are grateful to Professor Leonid Kazanskiy (The Institute of Physical Chemistry and Electrochemistry of Russian Academy of Science) for the assistance in the XPS investigations.

This work is supported by Russian Foundation of Basic Research (project 09-03-00554-a).

References

1. Hampson NA, Lee JB, Morley JR (1971) Electrochim Acta 16:637
2. Clarke TG, Hampson NA, Lee JB, Morley JR, Scanlon B (1969) Ber Buns Phys Chem 73:279
3. Becerra JG, Salvarezza RC, Arvia AJ (1990) Electrochim Acta 35:595
4. Alonso C, Salvarezza RC, Vara JM, Arvia AJ (1990) Electrochim Acta 35:489
5. Ambrose J, Barradas RG (1974) ElectrochimActa 19:781
6. Teijelo ML, Vilche JR, Arvia AJ (1984) J Electroanal Chem 162:207
7. Tilak BV, Perkins RS, Kozlovska HA, Conway BE (1972) Electrochim Acta 17:1447
8. Vidovich GL, Leikis DI, Kabanov BN (1962) Doklady Akademii Nauk SSSR 142:109
9. Droog JMM (1980) J Electroanal Chem 115:225
10. Doubova LM, Daolio S, Pagura C, De Battisti A, Trasatti S (2002) Russian J Electrochem 38:20
11. Savinova ER (2006) Razmernye i strukturnye effekty v elektrokatalize. Dissertation, Novosibirsk, Russia
12. Savinova E, Zemlyanov D, Pettinger B, Scheybal A, Schlogl R, Doblhofer K (2000) Electrochim Acta 46:175
13. Nechaev IV, Vvedenskii AV (2008) Sorbtsionnye I khromatograficheskiye protsessy 8:753
14. Nechaev IV, Vvedenskii AV (2009) Prot Met Phys Chem Surf 45:137
15. Marshakov IK, Vvedenskii AV, Kondrashin VY, Bokov GA (1988) Anodnoye Rastvoreniye i Selektivnaya Korroziya Splavov. VSU, Voronezh
16. Pickering HW (1968) J Electrochem Soc 115:143
17. Kaiser H. (1987) Chem Industries, Corrosion Mechanism. New York, Basel, 28: 85
18. Kaesche H (1979) Die Korrosion der Metalle. Springer Verlag, Berlin, Heidelberg, New York
19. Kuznetsova TA, Flegel' EV, Vvedenskii AV (2002) Prot Met 38:333
20. Kudryashov DA (2008) Anodnoye formirovaniye i svoistva nanoplyonki oksida Ag(I) na poli-, monokristallakh serebra i Ag, Au-splavakh. Dissertation, Voronezh, Russia
21. Vvedenskii A, Grushevskaya S, Kudryashov D, Kuznetsova T (2007) Corros Sci 49:4523
22. Forty AI, Rowlands G (1981) Phyl Mag 43A:171
23. Poate IM (1980) Gold Bull 14:2
24. Roldugin VI (2008) Fizikokhimiya poverkhnosti. Intellect, Moscow
25. Kapusta S, Hackerman N (1980) Electrochim Acta 25:1001
26. McAleer JF, Peter LM (1980) Farad Discuss Chem Soc 70:67
27. Collisi U, Strehblow HH (1990) J Electroanal Chem 284:85
28. Bard AJ, Stratmann M, Licht S (eds) (2002) Encyclopedia of electrochemistry. V.6: Semiconductor electrodes and photoelectrochemistry. Wiley-VCH, Weinheim
29. Zoski CG (ed) (2007) Handbook of electrochemistry. Elsevier, New Mexico State University
30. Pleskov YV, Gurevich YY (1986) Semiconductor photoelectrochemistry. Consultant Bureau, New York
31. Oshe EK, Rozenfel'd IL (1978) Itogi nauki I tekhniki. VINITI. Korroziya i zaschita ot korrozii: 111
32. Finklea HO (ed) (1988) Semiconductor electrodes. Elsevier, New York
33. Kudryashov DA, Grushevskaya SN, Vvedenskii AV (2007) Kondensirovannye sredy I mezhfaznye granitsy 9:53
34. Kudryashov DA, Grushevskaya SN, Vvedenskii AV (2007) Prot Met Phys Chem Surf 43:591
35. Vvedenskii A, Grushevskaya S, Kudryashov D, Ganzha S (2008) Surf Interface Anal 40:636
36. Luck'yanchilov AN, Grushevskaya SN, Kudryashov DA, Vvedenskii AV (2006) The environment for the photopotential measurement, Patent no. 55988 RF. Bulletin "Invitations. Useful models" 24: 3
37. Vvedenskii AV, Grushevskaya SN, Kudryashov DA, Luck'yanchilov AN (2007) The environment for the photocurrent measurement, Patent no. 66052 RF. Bulletin "Invitations. Useful models" 24: 3
38. Scheblykina GE, Bobrinskaya EV, Vvedenskii AV (1998) Prot Met 34:6
39. Kozaderov OA, Vvedenskii AV (2005) Prot Met 41:211
40. Wilson RH (1977) J Appl Phys 48:4292
41. Sutter EMM, Millet B, Fiaud C, Lincolt D (1995) J Electroanal Chem 386:101
42. Jiang ZY, Huang SY, Qian B (1994) Electrochim Acta 16:2465
43. Chatterjee K, Banerjee S, Chakravorty D (2002) Phys Rev B 66:854211
44. Kudryashov DA, Grushevskaya SN, Vvedenskii AV (2008) Prot Met Phys Chem Surf 44:301